# The BioCAT undulator beamline 18ID: a facility for biological non-crystalline diffraction and X-ray absorption spectroscopy at the Advanced Photon Source

**R. Fischetti,[a]‡ S. Stepanov,[b]‡ G. Rosenbaum,[c] R. Barrea,[a] E. Black,[a] D. Gore,[a] R. Heurich,[a] E. Kondrashkina,[a] A. J. Kropf,[c] S. Wang,[a] Ke Zhang,[a] T. C. Irving[a]* and G. B. Bunker[a]**

*[a]The Biophysics Collaborative Access Team (BioCAT), Department of Biological Chemical and Physical Sciences, Illinois Institute of Technology, Chicago, IL 60616, USA, [b]SER-CAT, University of Georgia, USA, and [c]CMT Division, Argonne National Laboratory, Argonne, Illinois, USA. E-mail: irving@biocat1.phys.iit.edu*

The 18ID undulator beamline of the Biophysics Collaborative Access Team at the Advanced Photon Source, Argonne, IL, USA, is a high-performance instrument designed for, and dedicated to, the study of partially ordered and disordered biological materials using the techniques of small-angle X-ray scattering, fiber diffraction, and X-ray absorption spectroscopy. The beamline and associated instrumentation are described in detail and examples of the representative experimental results are presented.

**Keywords: X-ray beamlines; non-crystalline diffraction; small-angle X-ray scattering; X-ray absorption spectroscopy; XAFS; XANES; EXAFS.**

## 1. Introduction

The Biophysics Collaborative Access Team (BioCAT) is organized as a NIH Biotechnology Resource dedicated to structural studies of partially ordered biological materials using small-angle X-ray scattering (SAXS), small-angle fiber diffraction, and X-ray absorption spectroscopy (XAS). It is located at sector 18 of the Advanced Photon Source (APS), Argonne National Laboratory, Argonne, IL, USA. The BioCAT facility is open to all researchers on the basis of peer-reviewed research proposals. Spectroscopy experiments include studies of metalloprotein solutions (with a special emphasis on small volumes and time-resolved XAS studies), oriented films, and oriented single crystals. X-ray scattering and diffraction studies that have been addressed include: macromolecular small-angle scattering, small-angle diffraction of muscle and connective tissue, oriented fibers of filamentous viruses, and various model membrane systems. The diversity of the BioCAT scientific program requires a flexible and high-performance X-ray beamline to achieve its goals. To this end, BioCAT has constructed and completed commissioning of an undulator-based beamline on sector 18 at the APS, which is the subject of this report.

## 2. Design rationale

The BioCAT beamline 18ID has been specifically designed to take advantage of the unique properties of undulator radiation from the APS – a third-generation machine similar to the European Synchrotron Radiation Facility (ESRF), Grenoble, France, and the Super Photon Ring-8 (SPring-8), Harima, Japan. Undulator sources on these machines can deliver a high flux into a small angular divergence with a small source size and, as such, are ideal for many of the scientific problems that the BioCAT facility is designed to address. In order to fulfill all the requirements of our experimental program, the beamline had to deliver a doubly focused undulator beam that could be scanned in energy over a wide range while maintaining a fixed position on the sample.

By employing highly demagnifying optics with independent horizontal and vertical focusing it is possible to match the beam dimensions at the sample and detector for a particular experiment – an important feature for fiber diffraction experiments. A high-energy-resolution ($\Delta E/E \simeq 10^{-4}$) scanning monochromator is needed to allow XAS experiments that span the $K$ edges of the first-series transition metals (particularly Mn–Zn, $\sim$6.5–10.5 keV), many of the $L_{\rm III}$ edges of the rare earth elements and gold and mercury. Calcium is a very important metal in biology and marks the low end of the energies targeted ($K$ edge $\sim$4 keV). Molybdenum ($K$ edge $\sim$20 keV) and cadmium ($K$ edge $\sim$27 keV) are also important elements for biological XAFS. The high-energy limit of the beamline is 35 keV, unless harmonics are used. High flux delivered into a small spot size is required for many practical time-resolved XAFS experiments and high-throughput modes that employ flow systems. Small focal spots ($\lesssim$ 100 µm in the vertical direction) are also required to exploit novel XAFS detectors developed by BioCAT (Zhang *et al.*, 1998, 1999; Karanfil *et al.*, 2000).

## 3. Beamline layout

The BioCAT beamline 18ID was designed by Dr G. Rosenbaum (currently with SER-CAT, University of Georgia, USA) and shares the same overall mechanical design as the SBC beamline 19ID. Undulator A (Lai *et al.*, 1993; Dejus *et al.*, 1994) was chosen as a source of very intense monochromatic radiation in the ranges 3.2–14 keV (first harmonic) and 9.6–42 keV (third harmonic). This device has very low angular divergence [$<$12 µrad (vertical) and $<$26 µrad (horizontal) FWHM] with a very small source size [typically $\sim$34 µm (vertical) by $\sim$636 µm (horizontal) FWHM, specifications as of summer 2004]. The undulator gap can also be tapered to deliver a smooth energy range of the order of 1 keV but with a significant loss in peak intensity. The undulator gap may be scanned at rates of $\sim$1 mm s$^{-1}$ under beamline control, permitting XAS scans over a range of $\sim$1 keV in 20 s when the monochromator is made to scan synchronously with the undulator. A differential pump separates the beamline vacuum structure from the storage ring eliminating the need for any windows between the beamline and the storage ring. This permits experiments at energies down to 4 keV (Ca $K$ edge).

Fig. 1 shows a schematic drawing of the beamline optics. The X-ray beam travels from the right to the left in this figure. There are three lead-lined structures that enclose the beamline. The first enclosure to the right houses a beam-defining mask for the synchrotron radiation and bremsstrahlung radiation collimators. The second enclosure houses most of the beamline X-ray optics. The entire X-ray beam path is under ultrahigh vacuum until the beam exits the beamline in the third enclosure, where the experiments are performed.

The first optical element is a moveable mask with a fixed aperture of 4.2 mm × 2.1 mm. This mask serves to reduce the heat load on the first monochromator crystal. It also serves as a white-beam position monitor by using temperature differentials (measured by appropriately placed thermocouples) in the mask to determine the beam center.

‡ Present address: GMCA-CAT, Biology Division, Argonne National Laboratory, Argonne, Illinois, USA.

 DOI: 10.1107/S0909049504016760  

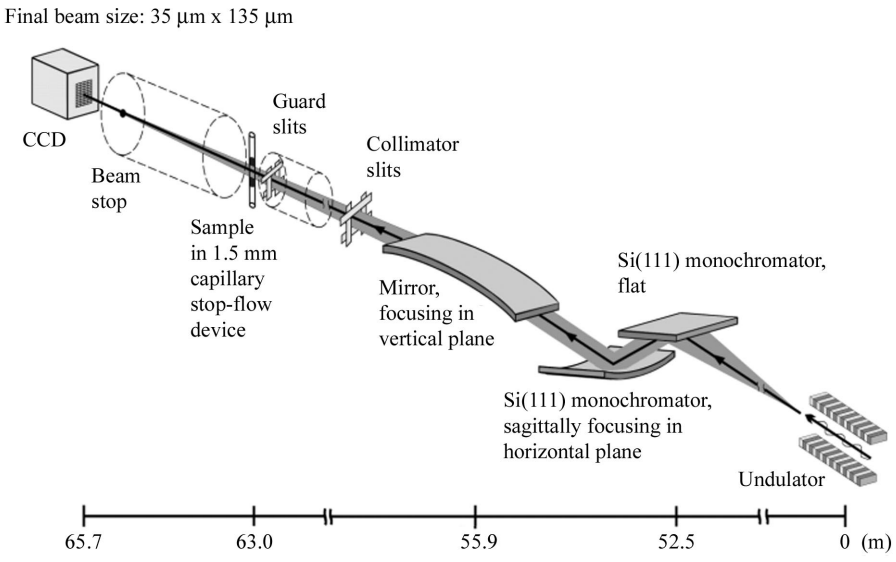


**Figure 1**
Schematic drawing of the beamline optics. The X-ray beam travels from the right to the left in this figure. The second monochromator with the Si(400) crystals is omitted for clarity and is located at 53.5 m from the source. The experimental arrangement shown is for a standard 2 m SAXS camera with a flow cell for solution scattering. Spectroscopy experiments are performed on a remotely actuated table located approximately 61.5 m from the source (not shown).

There are two independent double-crystal monochromators. The mechanisms are identical, but the upstream monochromator (52.5 m from source) has Si crystals with a (111) orientation while those in the downstream monochromator (54 m from source) have a (400) orientation. The user can select, under computer control, which monochromator they want to use based on the energy range or resolution desired. To preserve the fixed beam height and to keep the beam centered on the second crystal, both Bragg-normal and Bragg-parallel translations of the second crystal are under computer control. All motions are actuated by DC servomotors.

The cryo-cooled first crystal was designed as a collaborative effort between BioCAT, IMCA-CAT, MR-CAT, and SBC-CAT (Ivanov *et al.*, 2000). The crystal is supplied with liquid nitrogen using a Messer-Griesheim type-4 closed-loop pumping system connected to the liquid-nitrogen distribution system supplied by the APS. Both monochromators have sagittal-focusing second-crystal assemblies that can provide horizontal focusing of the beam. Because of the relatively small horizontal width of the beam impinging on the second sagittal-focusing crystal, it does not require stiffening ribs to minimize the effect of anticlastic bending. There is no loss of intensity when the beam is focused horizontally and near-theoretical spot sizes are achieved. We have observed an intensity profile of 140 μm FWHM after sagittal focusing at 12.0 keV at the focal point for a 2 m SAXS camera (about 64 m from the source) that corresponds to a demagnification ratio of 4.4:1. The maximum horizontal demagnification ratios are 6.2:1 and 7.3:1 for the first monochromator (upstream) and second monochromator (downstream), respectively. At the highest demagnification ratio, the smallest horizontal beam profile we have measured from the upstream monochromator was 115 μm (FWHM) at 12 keV.

The energy range of the upstream monochromator [Si(111) crystals] is 3.4–14.6 keV using the fundamental of the undulator spectrum. The experimentally determined rocking curve at 12 keV (FWHM = 36.4 μrad) agrees quite well with the theoretical curve (FWHM = 31.7 μrad) under these conditions. The measured photon flux in the focused X-ray beam at the sample position is $1.64 \times 10^{13}$ photons $s^{-1}$ at 12 keV and $2.23 \times 10^{13}$ photons $s^{-1}$ at 10 keV. The observed size of the unfocused monochromatic beam at the sample position is about 0.8 mm (vertical) by 3.6 mm (horizontal) as measured near the front of the experimental enclosure, 60 m from the source.

The downstream monochromator [Si(400) crystals] has an energy range of 7.9–33.8 keV. This range can be extended up to 67.6 keV by using the monochromator second harmonic [Si(800)] reflection. The experimentally determined rocking curve width for the Si(400) monochromator at 12 keV is 17.1 μrad (FWHM), which is comparable with the width of the theoretical rocking curve of 13.6 μrad (FWHM) under these conditions.

The beamline mirror (56 m from source) is used for harmonic rejection and vertical focusing and it can easily be withdrawn from and reset on the beam path as required. The mirror is constructed of ultralow expansion (ULE) glass-ceramic (Rocketdyne Corporation) of dimensions 1019 mm × 95 mm × 39 mm (L × W × H). As mounted in the bender, the mirror was measured to have a RMS slope error of 2 μrad over the central 800 mm of the mirror; the RMS surface roughness was 2–3 Å. The mirror surface is divided into three lanes: bare ULE, Pd-coated, and Pt-coated. The product of the energy and critical angle for the three surfaces is 30.51, 62.21 and 81.31 keV mrad for bare ULE, Pd-coated, and Pt-coated, respectively, enabling the mirror to cover the full energy range of the beamline. The mirror reflectivity is greater than 97% at the energies measured to date. The mirror can be used either flat or cylindrically bent to allow vertical focusing independently of any horizontal focusing. By applying an asymmetric couple, a smaller radius of curvature can be applied to the downstream end of the mirror, better approximating the ideal elliptical figure, leading to significant improvements in minimum vertical focus. When focused at the center of the front optical table (61.5 m from the source, demagnification ratio of 11.2:1) the beam profile has been observed to be as small as 35 μm (FWHM). The maximum convergence angles under these conditions are 0.16 mrad vertically and 0.19 mrad horizontally. Typical vertical beam profiles when focused for 1–6 m SAXS camera configurations range from 40 μm to 60 μm (FWHM). While these vertical focal spot sizes are well matched to the resolution of our detectors and are adequate for our current scientific program, they are larger than expected from the demagnification ratios and do not represent the best that can be achieved using current mirror technology. In the spring of 2005 the existing mirror and bender will be replaced with an adaptive 'Bimorph' mirror from Seso, which should produce a more ideal figure and yield smaller minimum focal spot sizes (8–10 μm FWHM) with less parasitic scattering.

Downstream of the mirror are horizontal and vertical beam-defining slits for the monochromatic beam. These can be set to pass the entire beam or define a beam as small as 25 μm × 25 μm. A monochromatic photon shutter allows the monochromator optics to stay warm while allowing the user to enter the experimental enclosure.

#### 4. Experimental enclosure

The third experimental enclosure is 12 m long × 5 m wide × 3.3 m tall. The first 2 m are taken up by the vertical collimation slits and the downstream support, which incorporates filter/shutter assemblies, and an ion chamber for the primary beam ($I_0$) monitor. Following the vertical collimation slits is a beryllium window (IF-1 grade, Brush-Wellman). All components upstream of this window are under high vacuum; downstream of the window all components are in a rough vacuum. The downstream support (59 m from the source) moves all of these components under computer control to follow the beam as it is reflected off the mirror. Immediately following the downstream support is a 1.2 m × 1.5 m optical table (60.5 m from the source), designed in collaboration with L. Rock Automation (Scottsdale, Arizona, USA) with 265 mm of rough vertical travel (1 µm resolution), 48 mm of fine travel (0.5 µm resolution), 40 mm of horizontal travel (1.7 µm resolution), and three degrees of rotational freedom. This table is used for most spectroscopy experiments as well as some diffraction experiments. Downstream of this table is a 6.4 m × 1.5 m vibration-isolation table (61.5–69 m from the source) that is used for most small-angle diffraction and scattering experiments. For convenience, the experimental enclosure has a rough vacuum manifold around its perimeter and it is well supplied with water, compressed air, and electricity. The 12 m length of the experimental enclosure allows for camera lengths from a few cm up to 6 m in order to fulfill the varied beam size and divergence requirements of a very broad range of small-angle X-ray diffraction and scattering experiments. The 5 m-wide enclosure offers ample room for ancillary equipment.

#### 5. Data acquisition and control

The beamline control software is based on the Experimental Physics and Industrial Control System (EPICS; http://www.aps.anl.gov/epics) which is a distributed system using VME-based electronics with crate controllers running the proprietary real-time UNIX-like operating system VxWorks (Wind River Systems). User interface software communicates with the VME crates over the Ethernet *via* the EPICS channel access (CA) protocol. The hardware is controlled by reading and writing the fields in the EPICS databases using CA calls from a wide variety of programming languages. The beamline graphical user interface (GUI) is implemented using Tcl/Tk and Java menus as well as using the EPICS graphical control displays (MEDM). These controls are all portable between different operating systems. The underlying beamline control and data-acquisition code, including fast on-the-fly scans, is written in C and is, therefore, portable between UNIX and Windows platforms. We have also developed a Perl software library that allows easy scripting of most of the beamline operations including multidimensional on-the-fly scans and time-resolved measurements. The portable beamline control software package *MX* (Lavender, 2000) is also supported.

The beamline motors and data-acquisition systems are controlled by four VME crates with Motorola MVME162FX crate controllers. The beamline motors were chosen to be DC servos because of their advantages in high torque, speed, and power consumption over stepper motors. Nine eight-channel Delta Tau PMAC-1 servo motor controllers control the beamline optics, the optical table, and *XY* positioning stages. For most of the experimental hutch equipment, stepper motors are used and controlled by four eight-channel Oregon Microsystems OMS-58 stepper motor controllers.

For the rapid energy scan mode (see §7 for a detailed explanation of our scan modes), data acquisition is performed by a Struck 7201 multichannel scaler with 32 inputs and 4k memory arrays per input. For other types of scans, including conventional step scans of various types, there is also a Joerger VCS16 scaler with 16 inputs and a voltage-to-frequency converter (Hytec VFC 2504, Hytec Electronics). External equipment (CCD detector, shutters) can be interfaced to the control system using a digital I/O board (Acromag-9440) with 16 input and 16 output channels. To implement PID feedback control loops there is also an Acromag IP330 ADC with 16 inputs and a Systran DAC with eight outputs.

There are four current amplifiers (Keithley model 42) and a Lakeshore temperature controller (model 330) for our cryostat (see below) that are interfaced through the RS232 ports on the beamline workstations. We have designed simulated EPICS servers for these devices so that they can be accessed from other computers in exactly the same way as the VME modules.

CAMAC modules can also be accommodated *via* Kinetic Systems KS-2917 VME to a CAMAC interface board and a Kinetic Systems CAMAC crate and model 3922 controller interfaced with EPICS. With this simple interface, user-supplied CAMAC devices can be quickly scripted and integrated into the beamline controls.

The CCD detectors (Phillips *et al.*, 2002) are controlled by a GUI-based program running on Windows NT/2000 and interfaced to the control system by a digital I/O line. The CCD control system has a built-in digital I/O and AD/DA capabilities provided by 12-bit National Instruments PCI boards that allow collection of multiple channels of additional data from the experiment tightly integrated with the area-detector data acquisition.

#### 6. Feedback systems

Stability of both beam position and intensity are extremely important at BioCAT. Samples are, in general, small (typically $<1$ mm, often $<0.1$ mm in one or more dimensions), the fluorescence detectors we use are sensitive to beam position, and there is the usual need to maintain the tune of the two crystals in the monochromator during energy scans.

For positional feedback, we have implemented an in-vacuum beam-position monitor (BPM) that was developed by the SBC-CAT (Alkire *et al.*, 2000). This BPM is linear over a range of a few millimeters and has a resolution of less than 2 µm. By using this BPM and a feed-forward approach to adjust the beam angle, we have been able to maintain a constant exit height to $<\pm 25$ µm over an XAS scan. In addition, a variable offset in the equations of motion of the monochromator conditions has been used to minimize energy-dependent beam-position changes.

To maintain beam intensity during energy scans, we have installed an analog feedback system to drive a piezo-electric actuator controlling the angle of the second crystal of the monochromator. A lock-in amplifier (Stanford Research Systems model SR830 DSP) and a custom-designed analog electronic feedback control unit complete the system. A small-amplitude sine wave of frequency $f$ is fed to the piezo actuator to impose a periodic variation on the beam intensity. When the two crystals are misaligned, but not more than one or two rocking-curve widths away from the diffraction condition, the lock-in amplifier will detect the intensity signal with frequency $f$ with a signal strength proportional to the slope of the rocking curve. With the proper choice of phase angle, the sign of this correction signal will indicate the direction to drive the piezo in order to recover peak intensity. The correction signal is fed into an integrator, the output of which is summed with the dither sine wave and a manually adjustable offset, and then transmitted to the piezo amplifier. When the peak intensity is achieved, *i.e.* crystals aligned, the intensity fluctuations will no longer have frequency $f$ but instead $2f$ resulting in no

correction signal. An amplitude for the dither signal of about 20% of the FWHM of the rocking curve is sufficient to drive the second crystal to the peak. The feedback system is capable of maintaining peak intensity for energy changes at a rate of 200 eV $s^{-1}$, allowing monochromator scans of 1000 eV in 5 s without losing intensity.

### 7. Rapid-scanning capability

To take full advantage of the high X-ray flux provided by the APS, the undulator and focusing optics of the beamline and, at the same time, to reduce radiation damage to labile biological samples, fast on-the-fly scanning software was implemented for beamline alignment and data-acquisition procedures. The fast continuous scans, in opposition to conventional step scans, allow reduction of scan times from the order of many minutes to that of a few seconds and, thus, decrease exposure of samples to X-rays while increasing overall throughput of the beamline by about two orders of magnitude. This was a challenging task since synchronization of different hardware is required and the distributed control system imposes network latencies on the communication between different VME crates and the control workstations. Currently two types of continuous scans have been implemented, a 'generic' fast scan and an 'energy' fast scan.

The generic scan mode allows the user to scan any servo or stepper motor at the beamline while recording the output into any of 16 input channels of the Joerger scaler. The scan may use one of three different algorithms. The lower limit to the time resolution that is imposed by the network latencies is 5 ms for stepper motors and $\sim$120 ms per point. As a result, the typical generic scan time at the beamline is $\sim$15–60 s. These scanning protocols have been very useful in beamline diagnostic and alignment and have found use in various experimental protocols.

The fast energy scan, as implemented for both beamline monochromators, is simplified by the fact that the synchronization of crystal rotation and linear displacement in the double-crystal monochromator is handled by the PMAC controllers (which were designed for simultaneous multi-axis motions), so that the scan software program needs to deal with one combined pseudo-motor called 'energy'. This scan makes use of the 32 memory arrays in the Struck multichannel scaler which simultaneously record the monochromator encoder outputs and the X-ray intensities collected on the fly as energy is scanned over the desired range. The minimum time per point for this scan is less than 1 ms and the total scan time is typically 5–20 s depending on the energy range selected. We have also included synchronous motion of the beamline undulator into the energy scan protocols so that the energy of the two devices can be changed simultaneously. Finally, all the energy and generic scan modes provide for two- or three-dimensional scans with stepwise motion of the second and the third motors, respectively, retaining continuous scanning in the first dimension. The fast energy scan is used for all beamline spectroscopy and microbeam applications.

### 8. Facilities

#### 8.1. SAXS camera

For SAXS experiments, the beam is defined by the collimator slits described above. At 3 m downstream of these slits are the guard slits (JJ X-ray type-3 vacuum compatible) mounted on motorized horizontal and vertical translation stages. This allows for accurate positioning and profiling of the beam for diagnostic purposes. A number of different sample holders, either supplied by the user or BioCAT, can be mounted on horizontal and vertical translation slides with 100 mm of travel and capable of carrying up to 258 kg loads. Control of the sample-holder position is integrated with the detector control and data-acquisition systems as described below.

A number of different SAXS camera configurations can be accommodated on the 6.4 m $\times$ 1.5 m vibration isolation table. Various combinations of stainless steel and PVC flight tube sections allow for a range of sample-to-detector distances from 0.3 m to 6 m. The flight tubes can be moved in and out of position using overhead cranes. Mica windows are used throughout except for the rear exit window that is composed of 0.127 mm-thick Kapton film. The set-up routinely uses a 4 mm-diameter backstop with an integrated single-element PIN photodiode for transmission measurements.

#### 8.2. Shutters

Two XIA model PF2S2 filter assemblies contain a series of aluminium filters (in vacuum) that allow at least three decades of beam attenuation (at 12 keV) as well as two pneumatically activated shutters which are routinely used for exposure times of 0.5 s or longer. For shutter opening times of 3 ms or longer we have an NM Laser Products model LS055 shutter that can be operated in vacuum. We have also recently implemented a shutter capable of $<$350 µs minimum exposure time consisting of two electrically activated inclined blade-type shutters in series (model LS500, NM Laser Products). Accurate exposure times are selected by using a simple GUI interface to a program that issues the correct pulse sequence to a Kinetic Systems model 3655-LIA timing-pulse generator to open and close the individual LS500 units at the appropriate time taking into account the mechanical and electrical latencies in each unit.

#### 8.3. Area detectors

Three detectors are currently available for small-angle diffraction and scattering applications. The first is a BAS2500 off-line image-plate scanner (Fuji Medical Systems, Stamford, CT, USA) which is capable of scanning with either 100 µm or 50 µm pixels using a 16-bit (log) ADC system to deliver a dynamic range of about 30000:1. The instrument can use either 20 cm $\times$ 25 cm or 20 cm $\times$ 40 cm plates. The second is a 1024 pixel $\times$ 1024 pixel, 60 mm active area, CCD detector similar to the so-called 'Green' detector developed by E. Westbrook and colleagues (Naday *et al.*, 1994). The CCD chip has four-port readout allowing readout times of 4 s. The third is a high-sensitivity CCD detector designed specifically for synchrotron small-angle diffraction and scattering applications (Phillips *et al.*, 2002). It has an active area of 49.3 mm $\times$ 86.3 mm with 4k $\times$ 7k 12 µm pixels. The control system for this detector is designed to be very flexible, with most sequencing operations based in software rather than in hardware, making it relatively easy to customize the readout modes for particular purposes. High gain is achieved by using a 1:1 fiber optic coupler rather than a demagnifying taper. The software uses a client/server model with a Windows NT/2000-based client that communicates with a server computer over the TCP/IP network which performs the actual detector control. Both CCD detectors suffer from relatively small active areas and we are currently implementing motorized translation stages to allow optimal positioning of the detectors to cover a desired range of reciprocal space under computer control.

#### 8.4. Goniometers

We have one goniometer system comprising one-quarter $\chi$ segment (Huber 511) on a $\theta$–$2\theta$ assembly (Huber 404). We also have a Huber model 410 rotation stage, model 5203 tilt stage, and 5102 translation stage that can be assembled in various configurations for

custom goniometry. These have been used for polarized XAFS and diffraction from oriented systems, *e.g.* model membrane systems.

### 8.5. XAFS detectors

Transmission ionization chambers modified from the CHESS design (Advanced Design Consultants, Lansing, NY, USA) are available for incident flux and transmission measurement. Three options are provided for fluorescence detection: a single-element germanium solid-state detector (Canberra GL0110S), a multilayer analyzer array (MAAD; Zhang *et al.*, 1998, 1999), and bent Laue crystal analyzers (Karanfil *et al.*, 2000). Dilute systems ($\sim$1 m*M*) require the capabilities of the MAAD or bent Laue detectors. We have also implemented bent Laue crystal-based analyzers for experiments at the Cd edge (26.712 keV), Mo edge (20.0 keV), Fe *K* edge (7.111 keV), and at the Zn edge (9.631 keV). We have used these bent Laue analyzers at energies as low as the Mn *K* edge (6.54 keV). Crystal/slit combinations designed specifically for experiments near a particular absorption edge represent a cost-effective way of rejecting background in XAS experiments (see §9 below).

### 8.6. Other XAFS instrumentation

XAS measurements on biological samples are routinely performed at low temperature to reduce the radiation damage caused by the production of free radicals and also to reduce the damping effect of temperature in the EXAFS oscillations (Cramer, 1988). Nevertheless, in some cases it is desirable to measure the samples in solution at room temperature in order to characterize the dynamic changes in structure that bridge the static endpoints provided by crystallography and to avoid the artifacts that can be introduced by freezing. Furthermore, flow systems can reduce the duty cycle for a given measurement providing faster throughput of samples that will permit more elaborate types of experiments to be designed and executed than is possible using conventional approaches.

For low-temperature XAS experiments, a closed-cycle Displex cryostat (http://www.arscryo.com/displex.html) is available that uses high-pressure helium gas to produce temperatures down to 10 K. The Displex has a DMX-20 low-vibration interface and utilizes an exchange gas to transfer the heat from the sample mount to a cold finger; a bellows assembly decouples the interface from the cold finger. A Lakeshore model 330 controller regulates the Displex temperature under EPICS control. A dual syringe stopped-flow system has been implemented at BioCAT to allow the users to perform XAS experiments in either continuous-flow or stopped-flow mode (Zhang *et al.*, 2004). Briefly, during a continuous-flow experiment, the sample is made to flow back and forth in a Kapton tubing (1 mm and 1.05 mm inner and outer diameter, respectively) to minimize radiation-induced damage to the sample. The system can be loaded with an arbitrary amount of sample, with a minimum volume of 10 µl. A smooth flow as slow as 0.05 µl $s^{-1}$ can be sustained during the measurement with the maximum speed being 200 µl $s^{-1}$. Rapid mixing of enzymes and substrates can be triggered from the beamline control computer or from the stop flow control computer. When running at the top speed, the mixing time can be as short as 8 ms with an observation holder directly attached to a mixer. The stopped-flow chamber can be cooled to temperatures as low as 233 K in order to lengthen the lifetime of a reaction. A portable UV/Vis spectrometer (Ocean Optics model 2000) may be integrated into the stopped-flow device through optical fibers and lenses allowing optical spectra to be collected simultaneously with an XAS measurement.

## 9. Results and discussion

### 9.1. Performance for X-ray absorption spectroscopy applications

Routine low-temperature XAS experiments use the Displex cryostat. The sample holder was designed to support up to five samples and allows the user to move between samples and resume the experiment in less than 5 min without needing to warm up the cryostat chamber. Usually the samples are mounted in aluminium cells and then frozen by immersion in liquid nitrogen prior to mounting in the cryostat chamber. The cryostat has two exit windows, one facing the detector and the other used for sample exchange. The cryostat itself is mounted on an *x*–*y* stage that allows the user to raster scan the sample in two dimensions during the experiment. This feature has been demonstrated to be very useful when working with samples that are sensitive to radiation damage. The stop-flow system has also proved to be a versatile instrument for both time-resolved XANES studies (Kleifeld *et al.*, 2003) and continuous-flow experiments (Zhang *et al.*, 2004).

The combination of the highly focused beam and the large area detectors available at BioCAT allow measurement of dilute samples, $\sim$0.1 m*M* concentration in many cases. A typical scan time is 20–60 s and it is necessary to record $\sim$50 scans at this concentration to obtain adequate statistics; thus a total time of 20–60 min suffices to complete an XAFS spectrum for each sample with either frozen samples or using the flow system. Fig. 2 shows a representative EXAFS signal of protein samples ($\sim$0.3 m*M* Zn concentration) at low temperature using a Zn bent Laue analyzer detector.

### 9.2. Performance for small-angle fiber diffraction

An important design goal of the beamline and instrumentation was to obtain high-quality fiber diffraction patterns from complex biological materials such as muscle and connective tissue. These materials are frequently composed of a number of different macromolecular assemblies with similar long-spacing repeats. This leads to complex X-ray patterns with closely spaced diffraction spots and streaks. The performance of this instrumental arrangement has been reported elsewhere (Irving *et al.*, 2000; Irving & Fischetti, 2001). First-order resolution can be of the order of $\sim$1500 Å with order-to-order resolution in excess of 10000 Å with flux densities in excess of $10^{15}$ photons $s^{-1}$ $mm^{-2}$ for time-resolved experiments. The very small focal spots and excellent collimation allows measurement of weak

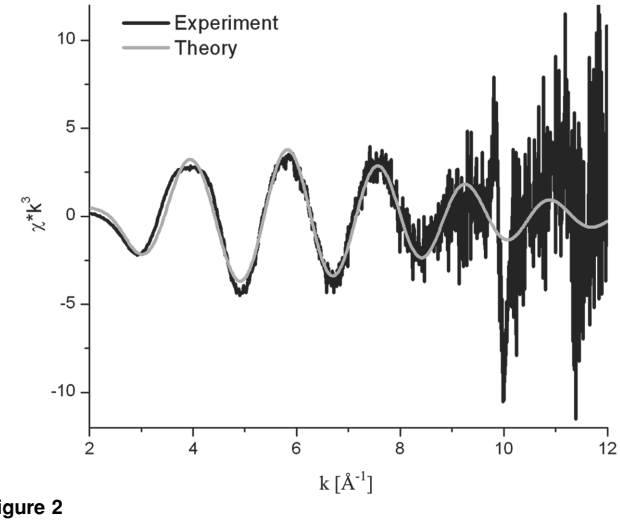


**Figure 2**
EXAFS signal of a $\sim$0.3 m*M* Zn membrane transporter measured at 30 K with the Zn bent Laue analyzer (Mijovilovich *et al.*, 2004, courtesy of Professor J. Penner-Hahn, University of Michigan, USA).

diffraction spots in the presence of high backgrounds enabling experiments on connective tissue (*e.g.* Orgel *et al.*, 2001) and muscle (*e.g.* Irving & Maughan, 2000; Reconditi *et al.*, 2004) that would be difficult or impossible using other instruments. Fig. 3 shows part of a diffraction pattern from gold-labeled rat-tail collagen showing the fine diffraction features that can be resolved in difficult systems using the 18ID optics and high-resolution area detectors.

### 9.3. Performance for SAXS

Small-angle X-ray scattering (SAXS) is a widely used technique for the measurement of the radius of gyration ($R$g), the electron pair distance distribution function [$P(r)$], and for *ab initio* modelling of low-resolution molecular envelopes of macromolecules in solution. The small focal spot sizes and high flux of the BioCAT beamline make it well suited for high-throughput testing of hypotheses concerning changes in macromolecular conformations with ligand binding or changing environmental conditions as well for time-resolved investigations of protein folding. The BioCAT standard experimental set-up includes a 2 m sample-to-detector-length camera to access a range of scattering wavevectors ($\mathbf{q}$) from $\sim$0.07 nm$^{-1}$ to 2.8 nm$^{-1}$ and a 0.3 m sample-to-detector-length camera for $\mathbf{q}$ in the range from $\sim$0.4 to 16 nm$^{-1}$ with the high-sensitivity CCD detector. This range of $\mathbf{q}$ permits reconstruction of molecular envelopes using any of a number of algorithms including spherical harmonic-based algorithms (Svergun & Stuhrmann, 1991), genetic algorithms (Chacon *et al.*, 1998), simulated annealing (Svergun, 1999), and "give 'n take" algorithms (Walther *et al.*, 2000). The standard sample chamber is a water-jacketed flow cell developed by Dr Xingwang Fang, University of Chicago, USA. The cell has a quartz capillary that requires less than 100 µl of sample. In order to reduce radiation damage (Fischetti *et al.*, 2003), the sample is flowed during exposure in the beam using a programmable dual syringe pump (Hamilton Microlab 540c). This cell design also allows mixing experiments to follow relatively slow processes (time scales of seconds to minutes). Using this set-up, small-angle scattering curves can be obtained in about 1 s with concentrations of protein as low as 0.3 mg ml$^{-1}$. Wide-angle measurements require somewhat higher concentrations, but satisfactory data can still be obtained from solutions as dilute as 2.5 mg ml$^{-1}$. An example of combined low- and wide-angle data from cytochrome *c* solution at 2.5 mg ml$^{-1}$ concentration is shown in Fig. 4 along with the theoretical scattering curve calculated from the known three-dimensional atomic structure of the protein using the *CRYSOL* program (Svergun *et al.*, 1995). The experimental results are in a good agreement with the calculations and demonstrate low instrumental background and the wide $\mathbf{q}$ range accessible when the data from the two camera lengths are merged. Useful low-$\mathbf{q}$ data have been obtained using somewhat longer times from as little as 0.3 mg ml$^{-1}$ protein. Rapid data acquisition enables the experimenter to screen a large number of samples or conditions in a given slot of beam time (*e.g.* Vigil, Blumenthal, Brown *et al.*, 2004; Vigil, Blumenthal, Heller *et al.*, 2004; Mehboob *et al.*, 2003; Telmer & Shilton, 2003) allowing more complex experiments to be contemplated than is usual at most existing facilities which are located on second-generation synchrotron sources. Furthermore, these rapid exposure times permit novel modes of data collection such as simultaneous liquid chromatography and SAXS measurements that may permit acquisition of interpretable data from unstable samples or multicomponent systems (Mathew *et al.*, 2004). A time resolution of about 3 ms in stopped-flow experiments (with total exposure times of 100 ms) using a stopped-flow device has also been demonstrated (Jacob *et al.*, 2004).

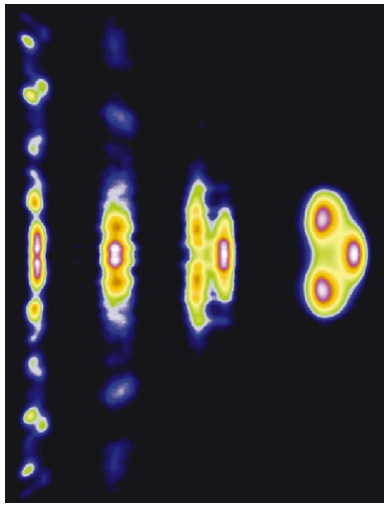

**Figure 3**
Off-meridional section of a background-subtracted diffraction pattern from gold-labeled rat-tail collagen fibers. Note the closely spaced but resolved diffraction spots on the lines showing the utility of the small focus in separating very weak signals from background noise. (Courtesy of Dr Joseph Orgel, Chicago Medical School, USA.)

### 9.4. Other experimental techniques

The beamline characteristics that make it ideal for small-angle diffraction and scattering have been shown to be advantageous for high-resolution fiber diffraction, *e.g.* from oriented gels of filamentous viruses (Parker *et al.*, 2002), and various general diffraction applications including powder diffraction from model membrane systems (*e.g.* Koynova & MacDonald, 2003). We have recently been commissioning a micro-emission spectroscopy set-up using a KB mirror system (KB Synchrotron Radiation-1, Xradia) and zone-plate-based technologies (Yun *et al.*, 1999). A description of these capabilities and initial results will appear elsewhere.

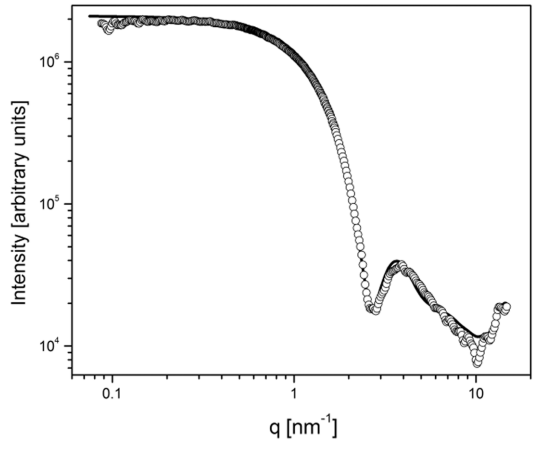


**Figure 4**
Experimental background-subtracted SAXS patterns (circles) measured from 2.5 mg ml$^{-1}$ solution of cytochrome *c* with the 2 m camera and 0.3 m camera combined into one curve. Exposure time was about 1 s with an incident flux of $\sim 2 \times 10^{13}$ photons s$^{-1}$. The corresponding SAXS curve calculated from the known three-dimensional atomic structure of cytochrome *c* using the *CRYSOL* program (Svergun *et al.*, 1995) is shown as a full line (calculation parameters: cytochrome *c* structure 1HRC from the Protein Data Bank, *CRYSOL* program used with 30 harmonics and other parameters set to defaults). The experimental and calculated results are in good agreement.

### 10. Future enhancements

There are a number of enhancements planned for the beamline hardware aimed at improving performance. We will be implementing vertical white-beam slits in 2004 to allow better beam diagnostics, to reduce the beam size, and to provide optimal illumination of the mirror. The existing mirror will be replaced in 2005 as described above. The experimental enclosure will be extended from 12 m to 15 m in late 2004 to allow three experimental set-ups to be left in place to minimize the set-up time when changing experimental modalities. Real-time positional feedback will be implemented to maintain the exit height to within $\pm 10$ µm during energy scans. Other enhancements are planned to allow automated beam alignment and focusing, greater flexibility of scanning software (scripts, graphics with data analysis capabilities, faster duty cycles for time-resolved experiments) and better integration of CCD detector software with the beamline controls.

We would like to thank Dr E. Westbrook (formerly of the Structural Biology Center, Argonne National Laboratory, and now with the Molecular Biology Consortium) for providing us with access to the SBC beamline drawings that were used as a basis for our design. Use of the Advanced Photon Source was supported by the US Department of Energy, Basic Energy Science, Office of Energy Research, under Contract No. W-31-109-Eng-38. BioCAT is a NIH-supported Research Center, RR08630.

### References

Alkire, R. W., Rosenbaum, G. & Evans, G. (2000). *J. Synchrotron Rad.* **7**, 61–68.
Chacon, P., Moran, F., Diaz, J. F., Pantos, E. & Anreu, J. M. (1998). *Biophys. J.* **74**, 2760–2775.
Cramer, S. P. (1988). *X-ray Absorption: Principles, Applications, Techniques of EXAFS, SEXAFS and XANES*, edited by D. C. Koningsberger and R. Prins, pp. 257–320. New York: John Wiley.
Dejus, R., Lai, B., Khounsary, A., Savoy, R., Moog, L. & Gluskin, E. (1994). Technical Bulletin ANL/APS TB-17. ANL, APS, Argonne, IL, USA.
Fischetti, R., Mirza, A., Rodi, D. J., Irving, T. C., Kondrashkina, E. & Makowski, L. (2003). *J. Synchrotron Rad.* **10**, 398–404.
Irving, T. C. & Fischetti, R. F. (2001). *Fibre Diffr. Rev.* **9**, 58–62.
Irving, T. C., Fischetti, R., Rosenbaum, G. & Bunker, G. B. (2000). *Nucl. Instrum. Methods*, A**448**, 250–254.
Irving, T. C. & Maughan, D. W. (2000). *Biophys. J.* **78**, 2511–2515.
Ivanov, I., Rosenbaum, G., Chrzas, J., Fischetti, R., Segre, C. U. & Chapman, L. D. (2000). *Synchrotron Radiation Instrumentation: Eleventh US National Conference*, edited P. Pianetta *et al.*, pp. 271–275. New York: American Institute of Physics.
Jacob, J., Krantz, B., Dothager, R. S., Thiyagarajan, P. & Sosnick, T. R. (2004). *J. Mol. Biol.* **338**, 369–382.
Karanfil, C., Zhong, Z., Chapman, L. D., Fischetti, R., Bunker, G. B., Segre, C. U. & Bunker, B. A. (2000). *Synchrotron Radiation Instrumentation: Eleventh US National Conference*, edited by P. Pianetta *et al.*, pp. 178–182. New York: American Institute of Physics.
Kleifeld, O., Frenkel, A. & Sagi, I. (2003). *Nature Struct. Biol.* **10**, 98–103.
Koynova, R. & MacDonald, R. C. (2003). *Biophys. J.* **85**, 2449–2465.
Lai, B., Khounsary, A., Savoy, R., Moog, L. & Gluskin, E. (1993). Technical Bulletin ANL/APS TB-3. ANL, APS, Argonne, IL, USA.
Lavender, W. M. (2000). *AIP Conf. Proc.* **521**, 332.
Mathew, E., Mirza, A. & Menhart, N. (2004). *J. Synchrotron Rad.* **11**, 314–318.
Mehboob, S., Jacob, J., May, M., Kotula, L., Thiyagarajan, P., Johnson, M. E. & Fung, L. W. (2003). *Biochemistry*, **42**, 14702–14710.
Mijovilovich, A., Liu, J., Mitra, B. & Penner-Hahn, J. E. (2004). In preparation.
Naday, I, Westbrook, E. M., Westbrook, M. L., Travis, D. J., Stanton, M., Phillips, W. C. & Xie, J. (1994). *Nucl. Instrum. Methods*, A**348**, 635–640.
Orgel, J. P. R. O., Miller, A., Irving, T. C., Fischetti, R. F., Hammersley, A. P. & Wess, T. J. (2001). *Structure*, **9**, 1–20.
Parker, L., Kendall, A. & Stubbs, G. (2002). *Virology*, **300**, 291–295.
Phillips, W., Stewart, A., Stanton, M. & Ingersoll, C. (2002). *J. Synchrotron Rad.* **9**, 36–43.
Reconditi, M., Linari, M., Lucii, L., Stewart, A., Sun, Y.-B., Boesecke, P., Narayanan, T., Fischetti, R. F., Irving, T., Piazzesi, G., Irving, M. & Lombardi, V. (2004). *Nature (London)*, **428**, 578–582.
Svergun, D. I. (1999). *Biophys. J.* **76**, 2879–2886.
Svergun, D. I., Barberato, C. & Koch, M. H. J. (1995). *J. Appl. Cryst.* **28**, 768–783.
Svergun, D. I. & Stuhrmann, H. (1991). *Acta Cryst.* A**47**, 736–744.
Telmer, P. G. & Shilton, B. H. (2003). *J. Biol. Chem.* **278**, 34555–34567.
Vigil, D., Blumenthal, D., Brown, S., Taylor, S. & Trewhella, J. (2004). *Biochemistry*, **43**, 5629–5636.
Vigil, D., Blumenthal, D., Heller, W., Brown, S., Canaves, J., Taylor, S. & Trewhella, J. (2004). *J. Mol. Biol.* **337**, 1183–94.
Walther, D., Cohen, F. E. & Doniach, S. (2000). *J. Appl. Cryst.* **33**, 350–363.
Yun, W., Lai, B., Cai, Z., Maser, J., Legnini, D., Gluskin, E., Chen, Z., Krasnoperova, A., Valdimirsky, Y., Cerrina, F., Di Fabrizio, E. & Gentili, M. (1999). *Rev. Sci. Instrum.* **70**, 2238–2241.
Zhang, K., Irving, T. C. & Auld, D. S. (2004). *J. Synchrotron Rad.* **11**, 204–208.
Zhang, K., Rosenbaum, G. & Bunker, G. (1998). *J. Synchrotron Rad.* **5**, 1227–1234.
Zhang, K., Rosenbaum, G. & Bunker, G. (1999). *J. Synchrotron Rad.* **6**, 220–221.

 Received 21 July 2003 • Accepted 8 July 2004 